Surface Charging and Impulsive Ion Ejection during Ultrashort Pulsed Laser Ablation

R. Stoian,* A. Rosenfeld, D. Ashkenasi,† and I. V. Hertel
Max-Born-Institut für Nichtlineare Optik und Kurzzeitspektroskopie, Max-Born Strasse 2a, D-12489 Berlin, Germany

N. M. Bulgakova
Institute of Thermophysics SB RAS, 1 Academician Lavrentyev Avenue, 630090 Novosibirsk, Russia

E. E. B. Campbell‡
Department of Experimental Physics, Göteborg University and Chalmers University of Technology, SE-41296 Göteborg, Sweden
(Received 24 August 2001; published 19 February 2002)

We report time-resolved studies using femtosecond laser pulses, accompanied by model calculations, that illuminate the difference in the dynamics of ultrashort pulsed laser ablation of different materials. Dielectrics are strongly charged at the surface on the femtosecond time scale and undergo an impulsive Coulomb explosion. This is not seen from metals and semiconductors where the surface charge is effectively quenched.

DOI: 10.1103/PhysRevLett.88.097603 PACS numbers: 79.20.Ds

The need for enhanced controllability and reduced collateral damage in laser micromachining is pushing femtosecond (fs) lasers to the forefront of material processing. Concomitantly, this has stimulated an increased interest in probing the nature of excitation, the dynamics of the energy redistribution in irradiated solids, and the precursor mechanisms for material removal [1]. Recently, the observation of fast ions in the initial, so-called gentle phase [2] of fs laser ablation of sapphire was reported, where ions of different mass have the same momenta. This was interpreted as originating from an impulsive, macroscopic Coulomb explosion (CE) of the charged dielectric surface [3]. Under conditions where this mechanism is dominant, the irradiated surface appears smooth and material removal can be accurately controlled on the nm scale [2]. This has been termed the gentle ablation phase. After a number of incubation pulses the ablation behavior changes (to what has been termed the strong phase [2]), an order of magnitude more material is removed per laser pulse, the majority of ions are slower, and the emitted species tend to have the same kinetic energy [3]. Here, we explore the dynamics of the initial stages of excitation in solids leading to charging, heating, and material expulsion and emphasize the material-dependent competition between nonthermal and thermal mechanisms. The excitation, energy redistribution, and material removal dynamics are studied by fs pump-probe techniques where the positive ion and electron emission is monitored as a function of the delay between two subthreshold 100 fs, 800 nm laser pulses. We compare the behavior of dielectrics, semiconductors, and metals. We find confirmation of the CE mechanism for dielectrics and quantify the magnitude and time scale of the charging process.

A Ti:sapphire laser beam was divided into two beams with equal energies that lay just below the ablation threshold for the second pulse [4]. The probe passed through a variable delay line and was then aligned collinear with the pump beam. Positive ion mass spectra or electron spectra were recorded with a time-of-flight (TOF) mass spectrometer as a function of the time delay between laser pump and probe. The charged particles were allowed to drift in a 65 mm field free region before they were extracted with a pulsed electric field with a variable delay (μs time scale) with respect to the laser pulses. The extraction field had a length of 9 mm. All ions (or electrons) present in this narrow region at the time of pulsing the extraction field were detected. (The shortest delay possible for the pulsed extraction voltage technique is 150 ns, corresponding to an electron kinetic energy of $\sim$0.5 eV.) By changing the delay time between laser pulse and electric field it is possible to map out an arrival time distribution for the ions at the extraction region. This can then easily be converted to an ion velocity distribution. Each laser pump-probe scan was carried out for a fixed delay of the electric field, i.e., for a narrow ion velocity range. The TOF distribution of the "prompt" electrons (see below) was measured by applying a negative bias to the sample and measuring the arrival time of the electrons at the detector without the application of any intermediate electric fields. The extraction grids of the spectrometer were arranged parallel to the substrate surface with a 25° incidence of the laser (measured with respect to the surface normal).

Figure 1(a) shows the TOF spectra of the electrons emitted from Al_2O_3 in the gentle phase (4 J/cm^2, 200 fs), normalized to the individual maxima. There are two contributions to the signal: prompt electrons [5], with energies on the order of eV, and slower (meV) plume electrons. The slow, plume electrons overlap in time with the positive ions (shown on the plot), and they can thus be regarded as plasma electrons, being trapped by the positive charge in the plume [3]. The prompt peak is shown on an expanded scale in Fig. 1(b). Here, the prompt electrons from Al_2O_3 are plotted, as are the prompt electrons from metallic Al (at 1.1 J/cm^2). The arrival time of the electrons from Al_2O_3 is

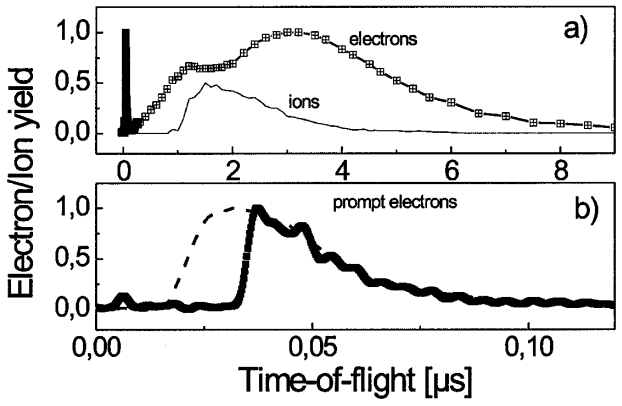

FIG. 1. Electron and ion TOF data for Al_2O_3. (a) Full range. Squares: both prompt electrons and slow, plasma electrons. Solid line depicts the TOF of the corresponding positive ions ($O^+ + Al^+$). (b) Expanded scale showing prompt electrons. Squares (thick line): from Al_2O_3; dashed line: from Al.

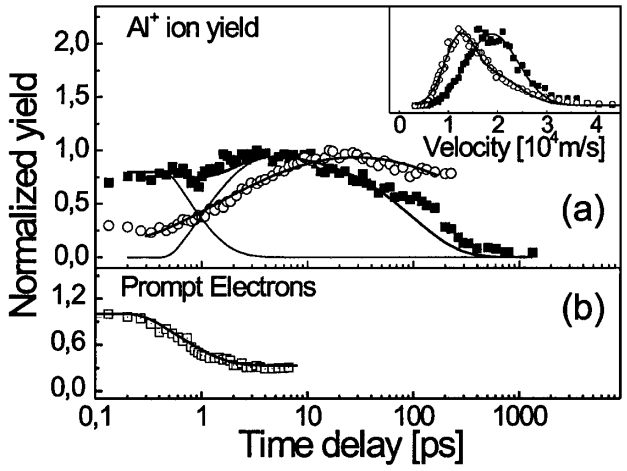

FIG. 2. Pump-probe measurements on Al_2O_3 (a) Al^+ yield as a function of delay between two equal, subthreshold 100 fs pulses. Squares: "fast" ions with a velocity of 2×10^4 ms^{-1} showing a double-peak structure. Full lines are drawn to guide the eye. Circles: "thermal" ions with a velocity of 1.2×10^4 ms^{-1}. Inset: velocity distributions for Al^+ measured at two pump-probe delays: Circles: 12 ps; squares: 0.6 ps. (b) Prompt electron signal under the same pump-probe conditions.

delayed compared to the Al case due to surface charging. Kinetic energy analysis shows that the electron energies from Al_2O_3 (but not from Al) are lower than the applied bias voltage, clearly indicating surface charging effects. The prompt electron energies were determined by measuring their arrival time for different bias voltages.

The prompt electron peak is most likely due to photoemission and leads to neutrality breakdown and strong surface charging inducing the electrostatic surface breakup. Daguzan *et al.* [6] have associated such fast electrons, observed from quartz, with free carrier absorption in the conduction band and photoemission.

Pump-probe measurements for both prompt electron and Al^+ production from Al_2O_3 are shown in Fig. 2. The ion data were obtained by choosing two different velocity windows for the detected ions and scanning the pump-probe delay in both cases. The velocity windows were chosen to select fast, Coulomb exploded ions observed predominantly during the gentle ablation phase (2×10^4 ms^{-1}) and the slower, thermal plasma ions (1.2×10^4 ms^{-1}) seen predominantly during the strong ablation phase [3]. The pump-probe signal from the faster ions (squares) shows a double-peak structure, illustrated by the full lines drawn to guide the eye. The slower ions (circles) have a single, broad peak at 20 ps. The ions within the first peak seen for the fast ions are present on a sub-ps time scale, too fast for a thermal mechanism to develop, they have mass-independent momenta [3], and have been associated with an impulsive electrostatic ejection. The inset shows the ion velocity distributions measured at pump-probe delays of 0.6 and 12 ps, respectively, confirming high velocities for the ions appearing at short pump-probe delays and a shifting of the distribution towards slower velocities for long delays. The second peak from the fast ion signal is due to the high energy tail of the thermal ions. The pump-probe data are not directly related to the time of ejection but give information on the time scale for energy coupling and redistribution within the sample. It can be seen from Fig. 2(b) that the prompt electron pump-probe data correlate very well with that of the first peak in the fast ion signal, indicating that prompt photoemission is indeed the origin of the observed ion CE. The prompt electron photoemission rate decreases on a time scale of 1 ps due to the relaxation of the highly excited free electrons created by the first laser pulse in the conduction band of Al_2O_3. If the hot electron population produced by the pump pulse decays, transferring electronic energy to lattice excitation, there may not be sufficient charging from the second laser pulse to produce the macroscopic surface CE. The thermal ions appear on the ps time scale given by the electron-phonon coupling and subsequent increase in the lattice temperature followed by heat dissipation, thus confirming the picture of the excitation and relaxation dynamics.

Pump-probe measurements of the Si^+ ions produced from a-SiO_2 behave similarly, as shown in Fig. 3(a), with fast CE ions observed for sub-ps delays as before. The main difference compared to Al_2O_3 is that the thermal ions onset for an earlier time delay. This is consistent with the fast (150 fs) electron relaxation and self-trapping in fused silica leading to an efficient early transfer of energy to the lattice [7].

The situation is different for Si and Au samples [Fig. 3(b)]. We observe almost no fast ions from Si within the sub-ps delay range of the CE peak for our conditions (pump fluence 80% of the single-shot ion emission threshold). Instead, we see an increased positive ion yield when the Si lattice has thermally melted, on the time scale of 4–10 ps, in very good agreement with time-resolved x-ray diffraction detection of the thermal response of the

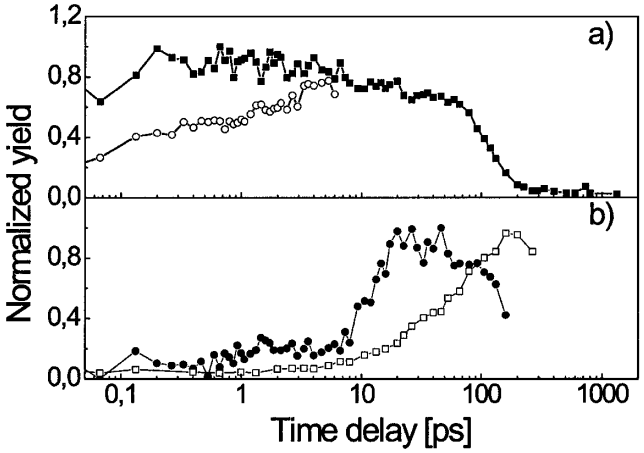

FIG. 3. (a) As Fig. 2(a) but yield of Si^+ from a-SiO_2; (b) pump-probe measurement for positive ion emission from Si (full circles, 0.45 J/cm^2 per pulse) and Au (open squares, 0.5 J/cm^2 per pulse). The data have been normalized to the same maxima.

Si lattice [8]. The ion emission on this time scale can be explained by the more efficient photon energy coupling in molten Si compared to solid material.

Figure 3(b) also shows the results of pump-probe measurements on a 1 μm thick Au film on quartz. Again, we have not found any evidence of CE from the Au film. As for Si, the ion yield is enhanced after the surface has melted on the 10–100 ps time scale. Recent results on the pump-probe dynamics of fs ablation of metals (Al, Fe, and Ni) have shown similar ion emission for delay times on the 10–20 ps time scale attributed to the development of a liquid surface layer [9]. This time is expected to be longer for Au due to the lower electron-phonon coupling [19].

To explain the observed behavior we have calculated the electronic dynamics including surface charging effects for Al_2O_3, Si, and Au. The bulk substrate is divided into layers each of depth 5 Å and the time dependence of charging and relaxation is calculated for each layer using appropriate boundary conditions. For the purposes of this Letter we are mainly interested in the induced charge at the outer layer of the bulk material. Other plasma-related effects such as the spatial charge distributions and the buildup of a double layer within the bulk material do not play an important role for the macroscopic CE discussed in this Letter but will be described in detail in a forthcoming publication. We use a slightly different approach for metals compared to dielectrics and semiconductors.

For Al_2O_3, we write the continuity equation for free electrons generated by the laser pulse as

$$\frac{\partial n_e}{\partial t} + \frac{1}{e}\frac{\partial J}{\partial x} = (\sigma_6 I^6 + \alpha n_e I)\frac{n_a}{(n_a + n_i)} - R_e - \mathrm{PE}, \quad (1)$$

where $\sigma_6 I^6$ is the rate of multiphoton ionization, n_x is the density of particles (a: neutral atoms, i: positive ions, e: electrons), I is the laser intensity, J is the electric current density, $\alpha n_e I$ is the avalanche term, R_e is the recombination term, and PE is photoemission. The rate of multiphoton ionization and the avalanche coefficient were based on a fit to the experimental results for the optical damage thresholds at different pulse durations [4] following a similar approach to [10] (taking into consideration the observed decay in the threshold electron density at longer pulse durations [11]) and estimated for Al_2O_3 with $\sigma_6 = 8 \times 10^9$ cm^{-3} ps^{-1} (cm^2/TW)^6 and $\alpha = 6$ cm^2/J.

The spatially and temporally dependent laser power inside the dielectric is determined by the optical response of a free electron plasma and the vacuum-plasma interface, being given by the complex dielectric function and Fresnel formulas [10,12] with a damping term $\omega\tau = 3$ to match reflectivities of 70% for supercritical electron densities [13]. We consider a statistical distribution of free electronic momenta in a wide band-gap dielectric, where the vacuum level is close to the conduction band minimum and only electrons with a momentum component normal to and in the direction of the surface can escape. Thus, we assume that on average half of the free electrons produced by multiphoton ionization and avalanche are immediately photoemitted from the top surface layer. Maximum photoemission occurs from the surface and decreases exponentially towards the bulk giving the photoemission term

$$\mathrm{PE} = \frac{1}{2}(\sigma_6 I^6 + \alpha n_e I)\frac{n_a}{(n_a + n_i)}\exp\left(-\frac{x}{l}\right) \quad (2)$$

with the electron escape depth, $l = 1$ nm [14].

The hole density is given by a similar equation as (1) disregarding photoemission. Hole transport is negligible for dielectrics. The current density is then described as

$$J = -en_e\mu_e E - eD\nabla n_e \quad (3)$$

with the electron mobility $\mu_e = 3 \times 10^{-5}$ m^2/(V s) (10 times lower than reported in Ref. [15] for a better match to the measured diffusivities [16]). The drift term was calculated using the Poisson equation. Since we consider transport in the local electric field, calculated from the Poisson equation, plasma screening effects within the bulk material are automatically accounted for. The diffusion coefficient $D = k_B T_e \mu_e / e$ is considered to be negligible for dielectrics compared to semiconductors and metals.

We use basically the same approach as described above for Si. We consider both one- and two-photon ionization. The cross sections for photoionization were taken from Ref. [12] as was the reflection coefficient. We consider both the electron and the hole current density [$\mu_e = 0.15$ m^2/(V s); $\mu_h = 0.045$ m^2/(V s)]. The photoemission term was treated analogously to that for metals [17,18]; see below.

The metallic case is considered as a plasma with a supercritical electron density. The system of equations used to describe the electric field generation consists of the heat flow equation for electrons (4) [19] (lattice coupling was neglected on this short time scale), the equation for the

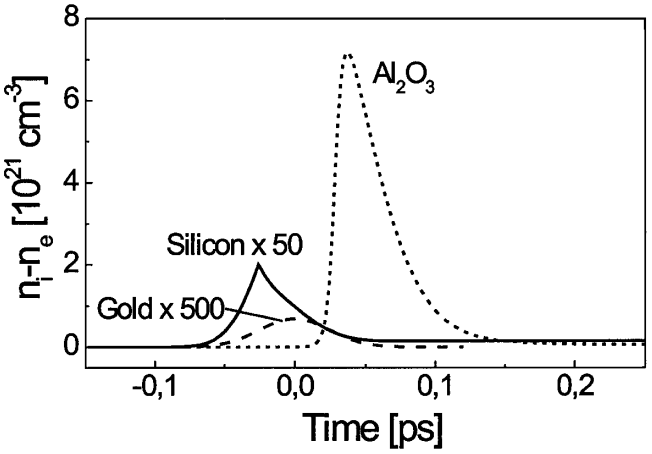

FIG. 4. Calculations of net surface charge density as a function of time for a laser fluence slightly above the one-shot ion emission threshold for each material. Laser pulse centered at $t = 0$ (FWHM = 100 fs). Note the change in the scales.

electric current density, the continuity equation (1) without source/sink terms, and the Poisson equation.

$$\frac{C_e}{T_e}\left(\frac{\partial}{\partial t}T_e^2 + \frac{J}{en_e}\frac{\partial}{\partial x}T_e^2\right) = \frac{K_{e,0}}{T_l}\frac{\partial^2}{\partial x^2}T_e^2 + 2S(x,t), \tag{4}$$

where T_e and T_l are the electron and lattice temperatures, respectively, and C_e is the electron heat capacity. $K_{e,0}(T_e/T_l)$, the thermal conductivity of the electrons, and the energy source term S are given as in [19]. The photoemission condition was given as $J_S = \eta S^3$ [17].

First results of the modeling are shown in Fig. 4 where the buildup of the net positive charge on the surface of Al_2O_3, Si, and Au targets is plotted as a function of time. The Gaussian laser pulse is centered at $t = 0$ with a FWHM of 100 fs. The laser fluences used to calculate the charging dynamics are slightly above the experimental ion emission threshold [4,12]. It is clear that the net charge is much larger for the dielectric target than for the metal or semiconductor. Sufficient charge can be accumulated at the dielectric surface to initiate CE on the 100 fs time scale. With semiconductors and metals, the higher electron mobility and higher density of available free electrons ensure effective screening and a much smaller net positive charge accumulation during the laser pulse. This is not sufficient, by orders of magnitude, to induce a macroscopic electrostatic breakup of the outer layers of the substrate. The charging also shows quite different time behavior for Al_2O_3, being retarded, instead of roughly following the laser pulse envelope as for metals and semiconductors. If we estimate the magnitude of the electric field at the surface of Al_2O_3, due to the net accumulation of positive charge, and assume that this field exists for 50 fs (FWHM), we can estimate the velocity with which the CE Al^+ ions are emitted from the surface based on momentum conservation laws. This is 2.3×10^4 ms^{-1}, in excellent agreement with the experimentally determined values for Al_2O_3 [3].

In conclusion, we have studied, both experimentally and theoretically, the dynamics of electronic and lattice excitation and material removal in ultrafast laser ablation of dielectrics, semiconductors, and metals. Different dynamical behavior is observed that has important consequences for the mechanisms of material removal. In particular, it is possible to obtain a very high charging of dielectric surfaces that can lead to a macroscopic CE of the top surface layers. The calculations are in good agreement with fs pump-probe studies and measurements of velocity distributions of emitted ions.

*Also at National Institute for Laser, Plasma and Radiation Physics, 76900 Bucharest, Romania.
†Present address: LMTB, Schwarzschildstrasse 8, D-12489 Berlin, Germany.
‡Corresponding author.
Email address: f3aec@fy.chalmers.se

[1] See *Laser Processing and Chemistry,* edited by D. Bäuerle (Springer, Berlin, New York, 2000), 3rd ed., Chap. 13.
[2] D. Ashkenasi *et al.,* Appl. Surf. Sci. **120**, 65 (1997).
[3] R. Stoian *et al.,* Phys. Rev. B **62**, 13 167 (2000).
[4] D. Ashkenasi, R. Stoian, and A. Rosenfeld, Appl. Surf. Sci. **154–155**, 40 (2000).
[5] S. Amoruso *et al.,* Appl. Phys. Lett. **75**, 7 (1999).
[6] P. Daguzan *et al.,* Phys. Rev. Lett. **73**, 2352 (1994).
[7] P. Audebert *et al.,* Phys. Rev. Lett. **73**, 1990 (1994).
[8] A. Rousse *et al.,* Nature (London) **410**, 65 (2001).
[9] V. Schmidt, W. Husinsky, and G. Betz, Phys. Rev. Lett. **85**, 3516 (2000).
[10] B. C. Stuart *et al.,* Phys. Rev. B **53**, 1749 (1996).
[11] F. Quèrè *et al.,* Appl. Phys. B **68**, 459 (1999).
[12] K. Sokolowsky-Tinten and D. v. d. Linde, Phys. Rev. B **61**, 2643 (2000).
[13] D. v. d. Linde and H. Schüler, J. Opt. Soc. Am. B **13**, 216 (1996).
[14] S. C. Jones, A. H. Fischer, P. Braunlich, and P. Kelly, Phys. Rev. B **37**, 755 (1988).
[15] R. C. Hughes, Phys. Rev. B **19**, 5318 (1979).
[16] A. Miotello and M. Dapor, Phys. Rev. B **56**, 2241 (1997).
[17] E. M. Logothetis and P. L. Hartman, Phys. Rev. Lett. **18**, 581 (1967).
[18] J. H. Bechtel, W. L. Smith, and N. Bloembergen, Phys. Rev. B **15**, 4557 (1977).
[19] S.-S. Wellershof *et al.,* Appl. Phys. A **69**, S99 (1999).